Landscape and Urban Planning 130 (2014) 36–49

Contents lists available at ScienceDirect

Landscape and Urban Planning

journal homepage: www.elsevier.com/locate/landurbplan

Research Paper

Quantifying spatiotemporal patterns of urban impervious surfaces in China: An improved assessment using nighttime light data

Qun Ma[a,b], Chunyang He[a,*], Jianguo Wu[a,c], Zhifeng Liu[a,b], Qiaofeng Zhang[d], Zexiang Sun[a,b]

[a] Center for Human-Environment System Sustainability (CHESS), State Key Laboratory of Earth Surface Processes and Resource Ecology (ESPRE), Beijing Normal University, Beijing 100875, China
[b] College of Resources Science & Technology, Beijing Normal University, Beijing 100875, China
[c] School of Life Sciences and School of Sustainability, Arizona State University, Tempe, AZ 85287, USA
[d] Department of Geosciences, Murray State University, Murray, KY 42071, USA

HIGHLIGHTS

- VANUI improved accuracy of estimating impervious surface areas with NTL data.
- China's impervious surface areas increased by 6.54% per year between 1992 and 2009.
- Expansion of China's urban impervious surfaces exhibited pronounced regional differences.
- Three coastal regions accounted for 54.64% of China's impervious surfaces in 2009.
- Five of the six large expansion hotspots of impervious surfaces were in eastern China.

ARTICLE INFO

Article history:
Received 6 September 2013
Received in revised form 14 June 2014
Accepted 16 June 2014

Keywords:
Urban impervious surfaces
Nighttime light (NTL)
Vegetation Adjusted NTL Urban Index (VANUI)
NDVI
China

ABSTRACT

Quantifying the spatiotemporal patterns of impervious surfaces (ISs) is crucial for assessing the environmental impacts of urbanization. Nighttime light (NTL) data provide a new way of mapping urban IS on broad scales. However, the accuracy of this approach is currently low and thus further improvements are much needed. Here we have estimated the urban IS dynamics of China from 1992 to 2009 using the Vegetation Adjusted NTL Urban Index (VANUI), which combines NTL and Normalized Difference Vegetation Index (NDVI) data. With VANUI, we were able to quantify the spatiotemporal patterns of IS in China with a much higher accuracy than previous methods. Key to this improvement was VANUI's ability to alleviate the problem of saturation inherently associated with NTL data. Our study shows that the total urban IS area of China increased substantially from 10,614.23 km^2 in 1992 to 31,147.63 km^2 in 2009, at an annual increase rate of 6.54%. China's urban IS expansion exhibited pronounced regional differences, with six large "hotspot" areas where urban IS expanded most substantially. These hotspot regions accounted for 0.87% of China's total land area, but 37.66% of the total area of urban IS expansion during 1992–2009. Measures of urban IS are not only important for characterizing urbanization patterns and processes, but also essential for assessing ecological and environmental impacts of urbanization. Our results provide a valuable dataset and new insights for better understanding the speed and scope of China's recent urbanization, as well as for designing and developing sustainable cities in China and beyond.

1. Introduction

Impervious surfaces (ISs) in urban areas refer to human-made land covers through which water cannot penetrate, including rooftops, roads, driveways, sidewalks, and parking lots (Arnold & Gibbons, 1996; Weng, 2012). With rapid urbanization, increasing proportions of landscapes have been converted into IS (Sutton, Elvidge, Tuttle, & Ziskin, 2010). The proliferation of urban IS has

* Corresponding author. Tel.: +86 10 58804498; fax: +86 10 58808460.
E-mail addresses: mq-0127@163.com (Q. Ma), hcy@bnu.edu.cn (C. He), Jingle.Wu@asu.edu (J. Wu), hanboms@126.com (Z. Liu), robin.zhang@murraystate.edu (Q. Zhang), kindsnake@126.com (Z. Sun).

http://dx.doi.org/10.1016/j.landurbplan.2014.06.009
0169-2046/

resulted in a number of environmental problems, such as increasing urban runoff, decreasing groundwater recharge, reducing water quality, and contaminating aquatic environments through increasing overland flow with urban pollutants (Brabec, 2002; Pappas, Smith, Huang, Shuster, & Bonta, 2008; Wu et al., 2011; Wu, 2014). Urban IS also modify the heat energy balance, creating urban heat islands (UHI) (Buyantuyev & Wu, 2010; Oke, 1982). In addition, the expansion of urban IS reduces aquatic biodiversity and degrades wetlands (Goetz & Fiske, 2008). Therefore, urban IS have been considered an important factor impacting urban sustainability and attracted increasing research attention in recent decades (Arnold & Gibbons, 1996; Weng, 2012; Wu, 2010).

China has experienced unprecedented and rapid urbanization since the start of its economic reform in 1978 (Bai, Chen, & Shi, 2012; Wu, Xiang, & Zhao, 2014). More than half of the population of China (51.27%, or 690.79 million) lived in urban areas in 2011, an increase of urbanization rate reaching 31.11% during the 30 years since 1981 (National Bureau of Statistics of China, 2012). During the same period, land converted to built-up areas increased 4.86 times, reaching a total of 36,165 km^2 (Ministry of Housing & Urban-Rural Development of China, 2012). This rapid urban expansion was accompanied by a rapid growth in urban IS, which may have resulted in significant environmental consequences in China, including the loss of arable land (Liu, Liu, Zhuang, Zhang, & Deng, 2003; Tan, Li, Xie, & Lu, 2005), air and water pollution (Shao, Tang, Zhang, & Li, 2006), increased flood frequency (Weng, 2001), accelerated UHI development (Zhou et al., 2004), reduced biodiversity (Zhao et al., 2006), and other hydrological and ecological disturbances. To deal with these problems, we first need to accurately quantify the spatiotemporal patterns of China's urban IS.

IS quantification or mapping is based on either ground measurements or remote sensing technologies (Weng, 2012). Remote sensing-based approaches are widely used for their advantages in saving time and labor. For example, using SPOT-5 data and a support vector regression model, Leinenkugel, Esch, and Kuenzer (2011) estimated the change in IS in settlements of the Mekong Delta from 2005 to 2009. Deng, Fan, and Chen (2012) used Landsat TM/ETM+ images and a spectral mixture analysis method to map IS expansion in the Pearl River Delta of China from 1998 to 2008. Sexton et al. (2013) developed an empirical method for retrieving long-term continuous fields of IS in the Washington, DC – Baltimore, MD megalopolis from 1984 to 2010 based on Landsat TM images. However, high or medium spatial resolution images are not suitable for mapping the spatiotemporal patterns of urban IS at a national or global scale because of the cost of imagery and the time and labor needed for image preprocessing and interpretation (Lu, Tian, Zhou, & Ge, 2008).

The nighttime light (NTL) data obtained by the Defense Meteorological Satellite Program's Operational Linescan System (DMSP/OLS) have been closely correlated with several characteristics of urban settlements (Elvidge, Baugh, Kihn, Kroehl, & Davis, 1997; Imhoff, Lawrence, Stutzer, & Elvidge, 1997), including built-up areas (Ma, Zhou, Pei, Haynie, & Fan, 2012; Yang, He, Zhang, Han, & Du, 2013; Zhou et al., 2014), population density (Lo, 2001), electric power consumption (Amaral, Câmara, Monteiro, Quintanilha, & Elvidge, 2005; He, Ma, Liu, & Zhang, 2013), and carbon emissions (Doll, Muller, & Elvidge, 2000). Thus, the NTL data can provide an alternative or a supplemental approach to mapping urban IS at regional and global scales (Elvidge et al., 2007; Lu et al., 2008). However, the NTL data suffer from the problem of saturation, which makes the result of IS derived from the NTL data inaccurate within urban areas.

The Vegetation Adjusted NTL Urban Index (VANUI), which combines NTL and Normalized Difference Vegetation Index (NDVI) data, was first proposed by Zhang, Schaaf, and Seto (2013) to reduce the effects of NTL saturation and increase the variation of NTL signal within urban areas. VANUI has been shown to be highly positively correlated with urban IS (Zhang et al., 2013). Therefore, the primary objective of this study was to quantify the spatiotemporal patterns of urban IS in China using VANUI. To achieve this goal, we first preprocessed the NTL data and the NDVI data to improve their continuity and comparability. Then we calculated the VANUI values in urban areas based on these preprocessed data. Next, we obtained the actual percent impervious surfaces (PIS) in selected sites from high-resolution images available on Google Earth. After that, we developed linear regression models to estimate the urban PIS in China based on the VANUI data and the actual PIS data. Finally, we quantified the spatiotemporal patterns of urban IS in China from 1992 to 2009 using a geographical information system (GIS).

2. Study area and data acquisition

Six types of remote sensing data were used in this research: the NTL data, the Moderate Resolution Imaging Spectroradiometer (MODIS) 16-day NDVI composite data, the Advanced Very High Resolution Radiometer (AVHRR) 10-day NDVI composite data, high-resolution images available on Google Earth, land use/cover data, and Landsat thematic mapper (TM) data. The Version 4 DMSP/OLS NTL data from 1992 to 2009 were obtained from the National Oceanic and Atmospheric Administration (NOAA)/National Geophysical Data Center (NGDC) website (http://ngdc.noaa.gov/eog/dmsp/downloadV4composites.html, Accessed 28.12.12). The NTL datasets were acquired by five DMSP satellites (F10, F12, F14, F15, and F16), and annual composites were produced for each satellite using the highest quality data collected. The NTL data measured lights on the Earth's surface, such as those generated by human settlements, gas flares, fires, and illuminated marine vessels. Many constraints were used to exclude sunlight, moonlight, glare, clouds, and lighting features from auroras. Ephemeral events such as fires were also discarded (Elvidge et al., 1999, 2001). The NTL data were recorded as 6-bit digital numbers (DN) ranging from 0 (background) to 63 (brightest) by averaging the DN values of lights from cities, towns, and other sites with persistent lighting for the whole year (Cao, Chen, Imura, & Higashi, 2009). The NTL data were given in 30-arc-second grids, spanning −180 to 180 degrees in longitude and −65 to 75 degrees in latitude.

We first projected the global NTL datasets onto an Albers Conical Equal Area projection and resampled the datasets to a pixel size of 1 km, based on a nearest neighbor resampling algorithm. Then, we extracted the NTL datasets based on the administrative boundaries of China. However, the NTL dataset could not be directly used to estimate the dynamics of urban IS because of the lack of continuity and comparability resulting from the composition of multi-year and multi-satellite data without on-board calibration (Liu, He, Zhang, Huang, & Yang, 2012; Zhao, Ghosh, & Samson, 2012). To improve their continuity and comparability, we preprocessed the NTL datasets with three main steps (inter-calibration, intra-annual composition, and inter-annual series correction) using the approach proposed by Liu, He, et al. (2012). The preprocessed data from 1992, 2000, and 2009 were then selected for analyzing the urban IS dynamics together with NDVI data from the corresponding years.

Two NDVI products were used in this research: MODIS 16-day NDVI composite data for 2000, and 2009 and AVHRR 10-day NDVI composite data for 1992, at 1-km spatial resolution. The version 4 MODIS/Terra 16-day 1-km NDVI composite data (1-km MOD13A2) were obtained from the National Aeronautics and Space Administration (NASA)/Goddard Space Flight Center (GSFC) website (http://ladsweb.nascom.nasa.gov/data/search.html, Accessed 28.12.12). As the Level 3 product, the MODIS/Terra NDVI products were computed from the Level 2 daily surface reflectance

product (MOD09 series), which was corrected for molecular (including water vapor) and aerosol scattering, thin cirrus clouds, and ozone absorption (Fensholt, Rasmussen, Theis, & Mbow, 2009). The MODIS 16-day 1-km NDVI composite data were produced through the aggregation of the red (band 1) and near-infrared (band 2) from their native 250-m resolution via the MODIS Gridding and Aggregation Process (Tarnavsky, Garrigues, & Brown, 2008). Minimizing the contamination by clouds is crucial for producing accurate estimates of urban impervious surface area, and this was done using the constrained view angle-maximum value composite (CV-MVC) method in which the maximum NDVI value with the smallest view angle or the closest-to-nadir view for each pixel per 16-day composite interval was chosen (Gallo, Ji, Reed, Dwyer, & Eidenshink, 2004; Gu, Li, Huang, & Okin, 2009; Solano, Didan, Jacobson, & Huete, 2010). A detailed description of the MODIS 16-day 1-km NDVI composite data has been reported by Huete et al. (2002). In addition, taking annual means, although it could not completely eliminate cloud and shadow contamination by itself, further reduced NDVI data sensitivity to seasonal and inter-annual fluctuations, thus improving the accuracy of the estimates of urban impervious surfaces (IS) dynamics (Zhang et al., 2013).

The AVHRR 10-day 1-km NDVI composite data were obtained from the United States Geographic Survey (USGS) website (http://edc2.usgs.gov/1km/comp10d.php, Accessed 28.12.12). The data were radiometrically calibrated, precisely georeferenced, and corrected for atmospheric effects. The maximum value composite (MVC) method was used to choose the maximum NDVI value for each pixel per 10-day composite interval. This method also reduces the number of cloud-contaminated pixels and selects the pixels closest to nadir (Holben, 1986). A detailed description of the AVHRR 10-day 1-km NDVI composite data can be found on the USGS website (http://edc2.usgs.gov/1KM/paper.php#proc2). We also derived the annual mean NDVI values for this NDVI product, as per Zhang et al. (2013). Then we projected all the annual mean NDVI data onto an Albers Conical Equal Area projection and resampled the data to a pixel size of 1 km, based on the nearest neighbor resampling algorithm. After that, we extracted them according to the administrative boundaries of China.

The annual mean NDVI data for 1992, 2000, and 2009 could not be used directly to estimate the dynamics of urban IS because of the lack of consistency and comparability as a result of sensor degradation and discrepancies among different sensors. To reduce abnormal discrepancies and improve comparability, we preprocessed the annual mean NDVI datasets with two main steps (i.e., within- and among-sensor calibration). First, we selected the Taklimakan Desert as the calibration area because of its high conformity to NDVI values over different years, and then developed a linear regression model to calibrate the NDVI data from different years for the same sensor (Teillet & Holben, 1994). Second, we used the linear regression model proposed by Steven, Malthus, Baret, Xu, and Chopping (2003) for the inter-calibration of the NDVI data from different sensors. Readers are referred to Teillet and Holben (1994) and Steven et al. (2003) for details of the calibration procedures for the time-series NDVI data.

Google Earth images of high spatial resolution throughout China were used to obtain the actual PIS of the samples. These images often have a spatial resolution of less than 5 m, including Aerial Imagery, QuickBird, IKONOS, and SPOT. They contain rich spatial information on land covers (e.g., urban IS). Elvidge, Tuttle, and Sutton (2010) and Sutton, Elvidge, Baugh, and Ziskin (2011) indicated that Google Earth images are well suited for estimating actual PIS, although there are some compression-related distortions present in these images.

National land use/cover datasets (NLCD) of China for 1990, 1995, 2000, 2005, and 2010 were obtained from the Data Sharing Infrastructure of the Earth System Science website (http://www.geodata.cn/Portal/index.jsp, Accessed 27.01.14). The datasets were produced through the visual interpretation of Landsat Multi Spectral Scanner (MSS)/TM/Enhanced Thematic Mapper Plus (ETM+) and China-Brazil Earth Resource Satellite 1 (CBERS-1) images at 30-m spatial resolution, and then were converted into 1-km component grid datasets which contained detailed information of land use/cover in each pixel (Liu, Zhang, & Hu, 2012).

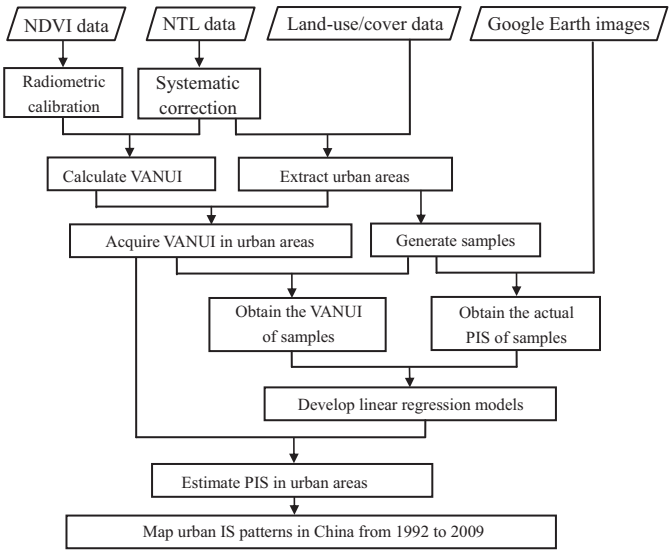

Fig. 1. Procedures for mapping the spatiotemporal patterns of urban impervious surfaces (IS) in China using a combination of fine- and coarse-resolution images.

Landsat TM images of high quality were obtained from the Geospatial Data Cloud website (http://www.gscloud.cn/, Accessed 27.01.14). The images covered the three mega-cities of Beijing, Tianjin, and Guangzhou with the acquisition time of 22 September 2009, 16 September 2009, and 2 November 2009, respectively.

The boundaries of administrative units were based on the National Geomatics Center of China at the scale of 1:4,000,000. Our study focused only on the mainland China although Taiwan, Hong Kong, and Macao were still present in the figures.

3. Methods

3.1. Estimating urban impervious surfaces over time

Our proposed method for mapping the spatiotemporal patterns of urban IS includes five steps (Fig. 1): (1) extract urban areas using the preprocessed NTL data and land use/cover data; (2) calculate VANUI in urban areas; (3) generate samples in urban areas and obtain their actual PIS; (4) develop linear regression models; (5) map the urban IS in China from 1992 to 2009. To recognize regional differences in geography and socioeconomic conditions, our study divided China into eight regions according to the Coordinated Regional Development Strategy and Policy Reports (Development Research Center of the State Council of China, 2005): Northeast China (NEC), Northern Coastal China (NCC), Eastern Coastal China (ECC), Southern Coastal China (SCC), the Middle Reaches of the Yellow River (MRYLR), the Middle Reaches of the Yangtze River (MRYTR), Southwest China (SWC), and Northwest China (NWC) (Fig. 2). All the steps were performed for each region.

3.1.1. Extracting urban areas

Urban areas refer to the places with intensive human activities and large areas of human-made land covers, including buildings, roads, industrial facilities, and parks (Kuang, Liu, Zhang, Lu, & Xiang, 2013; Potere & Schneider, 2007; Wang et al., 2012). We used the

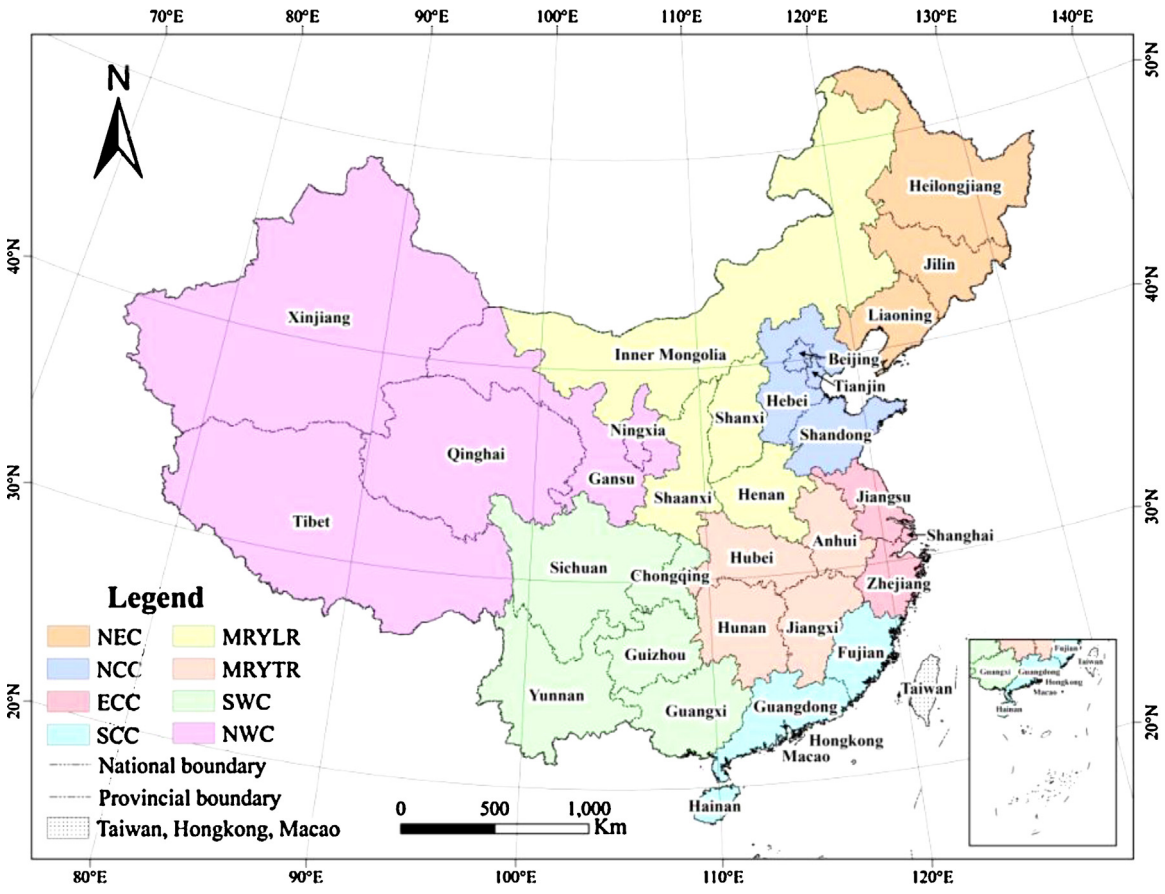

Fig. 2. Eight regions of China according to the Coordinated Regional Development Strategy and Policy Reports.

thresholding technique, developed by Liu, He, et al. (2012), to extract urban areas from 1992 to 2009 based on the preprocessed NTL data for 1992–2009 and the urban areas derived from the land use/cover data for 1990, 1995, 2000, 2005, and 2010. The threshold technique has been widely used to map urban areas due to its relatively high accuracy and simplicity (Henderson, Yeh, Gong, Elvidge, & Baugh, 2003; Imhoff et al., 1997; Milesi, Elvidge, Nemani, & Running, 2003). Optimal thresholds were determined when the urban areas extracted using the NTL data could best match the urban areas extracted using the land use/cover data with regard to the spatial extent. For each region, the thresholds for 1990, 1995, 2000, 2005, and 2010 were applied, respectively, to the years of 1992, 1993–1997, 1998–2002, 2003–2007, and 2008–2009. This method proved to be a useful way of extracting the dynamics of urban expansion in China (Liu, He, et al., 2012). The urban areas for 1992, 2000, and 2009 were selected for quantifying the urban IS dynamics in China.

3.1.2. Calculating VANUI in urban areas

We computed VANUI in urban areas for 1992, 2000, and 2009 using the following formula (Zhang et al., 2013):

$$\mathrm{VANUI} = (1 - \mathrm{NDVI})^{*}\mathrm{NTL}_{\mathrm{nor}}, \quad (1)$$

where NDVI is the annual mean NDVI derived from MODIS or AVHRR. The NDVI values were constrained to the range of positive values between 0 and 1.0 because negative NDVI values are usually associated with water and glaciers (Zhang et al., 2013). $\mathrm{NTL}_{\mathrm{nor}}$ is the normalized value of the preprocessed NTL data:

$$\mathrm{NTL}_{\mathrm{nor}} = \frac{\mathrm{NTL} - \mathrm{NTL}_{\mathrm{min}}}{\mathrm{NTL}_{\mathrm{max}} - \mathrm{NTL}_{\mathrm{min}}}, \quad (2)$$

where $\mathrm{NTL}_{\mathrm{min}}$ and $\mathrm{NTL}_{\mathrm{max}}$ are the minimum and maximum values in the NTL data (0 and 63, respectively).

The VANUI values ranged from 0 to 1.0. Central business districts (CBD) with little vegetation and a high lighting intensity had positive VANUI values close to 1, and peri-urban areas with lush vegetation and dim lighting had low VANUI values close to 0. The rationale behind using VANUI for urban IS estimation is that NTL data are positively correlated with IS, and vegetation abundance is inversely correlated with IS (Weng & Lu, 2008; Zhang et al., 2013). Thus the two types of data can be used together to improve the accuracy of estimating both the amount and spatial distribution of urban IS (Lu et al., 2008).

3.1.3. Generating samples and obtaining their actual PIS

There have been three common approaches to acquiring actual PIS of samples at a regional or global scale. The first approach is to directly use publicly available PIS products as actual PIS data (Elvidge et al., 2004, 2007). However, this approach does not work in China because public PIS products are generally unavailable. The second approach is to use the PIS derived from medium spatial resolution images as a surrogate (Lu et al., 2008). However, this approach is logistically challenging on a national scale because it is time-consuming for image preprocessing and interpretation. Plus, it often overestimates PIS in regions with extensive bare ground, while underestimating PIS in regions with a substantial amount of clouds and shadows (Lu & Weng, 2006; Wu & Murray, 2003). The third approach is to use Google Earth images to estimate actual PIS (Sutton et al., 2010, 2011). While also relatively time-consuming, this method is easy to implement on a national or global scale with relatively high accuracy (Elvidge et al., 2010).

For simplicity and convenience, our study used a method similar to the third approach to acquire the actual PIS in China. First, we randomly selected 700 sample plots (more than 80 sample plots for each region) with a window size of 1 km by 1 km in urban areas where no major changes in land use and land cover pattern took place between 1992 and 2009 – i.e., relatively stable regions – for developing robust regression models for different years. Then we evenly distributed 400 squares with a window size of 10 m by 10 m in each sample plot to capture its land cover characteristics. Second, all sample plots were exactly linked to the VANUI images for 1992, 2000, and 2009, respectively, to extract their VANUI values. Third, we converted all sample plots into a Keyhole Markup Language (KML) file and then loaded them into Google Earth. Finally, we selected Google Earth images of high quality in 2009 to determine the main land-cover type (e.g., building roof, street, road, tree, shrub, open area, and water) in each square, and the actual PIS in each sample plot was calculated by the fraction of 400 squares that were classified as IS.

3.1.4. Developing linear regression models

Linear regression models are widely used for estimating PIS at a regional or global scale because of their simplicity and relatively high accuracy (Elvidge et al., 2007; Kuang et al., 2013; Sutton et al., 2011). In each region, we randomly selected approximately 70% of the samples to develop a linear regression model and the rest for accuracy assessment. We developed linear regression models using the VANUI values of samples for 1992, 2000, and 2009 as the independent variable, respectively, and the actual PIS of samples derived from Google Earth images from 2009 as the dependent variable. The *F*-tests and coefficient of determination (R^2) were used to evaluate model performance. The *F*-test was used to examine whether the regression model was significant. The R^2 was used to measure the percentage of variation explained by the regression model.

3.1.5. Mapping the urban IS from 1992 to 2009

For each region, we applied the linear regression models and the VANUI values acquired from Section 3.1.2 to estimate the urban IS for 1992, 2000, and 2009. Finally, the urban IS in China from 1992 to 2009 were mapped out.

3.2. Quantifying the spatiotemporal patterns of urban IS

We first calculated the index of urban IS percentage (UISP) to quantify the patterns of urban IS in 2009 at national, regional, and provincial scales, with the following formula:

$$\mathrm{UISP} = \frac{\mathrm{UISA}}{\mathrm{TA}} \times 100\%, \tag{3}$$

where UISP is the urban IS percentage (%), UISA is the total urban IS area in a specific zone (km^2), and TA is the total area of a specific zone (km^2).

Then we characterized the changes of urban IS from 1992 to 2009 at national, regional, provincial, and county scales using the index of relative urban IS expansion index ($UISE_r$), with the following formula:

$$\mathrm{UISE}_r = \frac{\mathrm{UISA}_j - \mathrm{UISA}_i}{\mathrm{TA}} \times 100\%, \tag{4}$$

where $UISE_r$ is the relative urban IS expansion index (%), $UISA_i$ is the total urban IS area in the *i*th year (km^2), $UISA_j$ is the total urban IS area in the *j*th year (km^2), and TA is the total area of a specific zone (km^2).

At the county scale, we performed spatial autocorrelation analysis (Anselin, 1995; Goodchild, 1986) to identify the hotspot areas with high $UISE_r$, and then further characterized the growth patterns of urban IS in new urban areas within these hotspot areas for 1992–2009.

3.3. Accuracy assessment for the estimated urban IS in China from 1992 to 2009

We first used four statistical measures, namely the root-mean-square error (RMSE), mean absolute error (MAE), systematic error (SE), and correlation coefficient (*R*), to describe the differences between the estimated urban PIS and the actual urban PIS in each region for 1992, 2000, and 2009 (Hu & Weng, 2009; Xian & Homer, 2010). They were computed as follows:

$$\mathrm{RMSE} = \sqrt{\frac{\sum_{i=1}^{N}(\hat{I}_i - I_i)^2}{N}}, \tag{5}$$

$$\mathrm{MAE} = \frac{\sum_{i=1}^{N}|\hat{I}_i - I_i|}{N}, \tag{6}$$

$$\mathrm{SE} = \frac{\sum_{i=1}^{N}(\hat{I}_i - I_i)}{N}, \tag{7}$$

and

$$R = \frac{\sum_{i=1}^{N}(\hat{I}_i - \bar{I})}{\sum_{i=1}^{N}(I_i - \bar{I})}, \tag{8}$$

where $\hat{I}_i$ is the estimated urban PIS for sample *i*, I_i is the actual urban PIS for sample *i*, $\bar{I}$ is the mean value of the actual urban PIS for all samples, and *N* is the total number of samples.

Second, we used Google Earth images to examine whether the estimated urban PIS dynamics captured the actual details of urban

Table 1
Linear regression models for estimating urban IS in eight regions of China during 1992–2009.

Year	Model (PIS = $a + b$VANUI)	NEC	NCC	ECC	SCC	MRYLR	MRYTR	SWC	NWC
2009	*a*	−1.524	−1.719	−0.860	−0.661	−1.572	−1.034	−0.520	−2.729
	b	2.737	3.173	2.263	2.043	2.848	2.428	1.733	4.133
	R^2	0.687	0.810	0.789	0.668	0.630	0.652	0.657	0.724
	F-test	100.897	217.187	183.118	74.349	54.568	58.003	59.420	49.728
2000	*a*	−0.735	−0.865	−0.391	−0.387	−0.655	0.048	−0.052	−1.866
	b	1.841	2.060	1.651	1.581	1.751	0.992	1.170	3.101
	R^2	0.735	0.592	0.740	0.592	0.573	0.451	0.653	0.760
	F-test	127.578	62.577	139.820	53.598	43.000	25.498	58.222	60.257
1992	*a*	−0.562	−0.090	0.021	−0.202	−0.160	0.056	0.073	−0.976
	b	1.797	1.129	0.999	1.232	1.212	0.947	0.932	2.273
	R^2	0.675	0.447	0.500	0.334	0.608	0.356	0.359	0.419
	F-test	85.016	35.515	48.016	15.048	49.615	17.125	16.811	12.239*

* $P < 0.01$; for all others $P < 0.001$.
Note: PIS represents the fraction of impervious surfaces within a single pixel; R^2 represents the coefficient of determination for the evaluation of regression model performance.

PIS change in China from 1992 to 2009. Only high-resolution images since 1999 were used to evaluate the dynamics of urban PIS because of the time limitation of available images in Google Earth.

4. Results

4.1. Linear regression models for estimating urban IS

The linear regression models based on the index of VANUI and the actual PIS data performed well to estimate urban IS in China from 1992 to 2009 (Table 1). All of the developed linear regression models were significant based on the *F*-test at less than 0.001, except the linear regression model developed for NWC in 1992 (significant at 0.01). The values of R^2 of the developed linear regression models for each region were lager than 0.334, 0.451, and 0.630 for 1992, 2000, and 2009, respectively.

4.2. Urban IS in 2009

The estimated total UISA in China in 2009 was 31,147.63 km^2 (UISP = 0.33%), dominated by medium-intensity urban IS (Fig. 3). Of the total urban IS pixels, medium-intensity urban IS (30–70% PIS) made up 60.34%.

Urban IS in China showed large regional discrepancies (Fig. 4). From NWC to SWC, MRYLR, NEC, MRYTR, SCC, NCC, and ECC, UISP increased exponentially (Fig. 5). This discrepancy in urban IS was also pronounced at the provincial scale (Fig. 6). In particular, Beijing and Tianjin (in NCC) and Shanghai (in ECC) had much higher UISP, with values larger than 5%. The three metropolitan regions (equivalent to provinces) accounted for only 0.36% of China's total land area, but 12.40% of the total UISA in China. By comparison, the UISP of Inner Mongolia (in MRYLR), Gansu, Xinjiang, Qinghai, and Tibet (in NWC) were all less than 0.1%. These five provinces, covering 54.08% of China's total land area, accounted for only 7.72% of the total UISA in China.

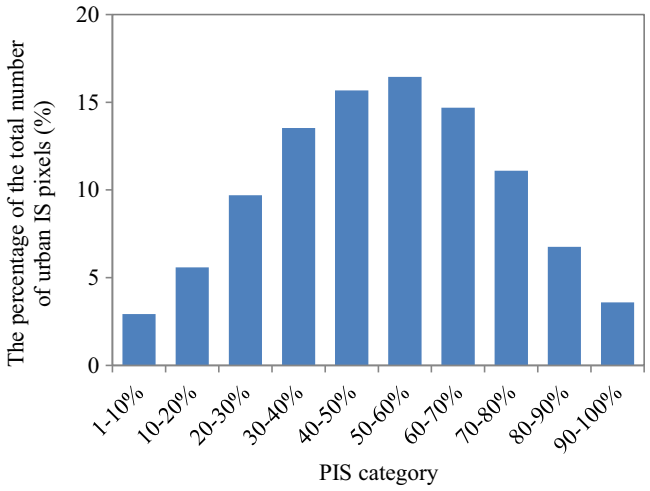

Fig. 3. Pixels of urban IS categorized by 10% interval in 2009, showing the distribution of percent impervious surfaces (PIS) category within the urban area.

4.3. Changes in urban IS from 1992 to 2009

Urban IS in China increased substantially during the study period. The total UISA increased from 10,614.23 km^2 in 1992 to 31,147.63 km^2 in 2009, with UISE$_r$ of 0.22%. The annual growth rate of urban IS in China from 1992 to 2009 was 6.54%, nearly 2 times the annual increase rate of urban population (3.95%) during the same period (National Bureau of Statistics of China, 2012).

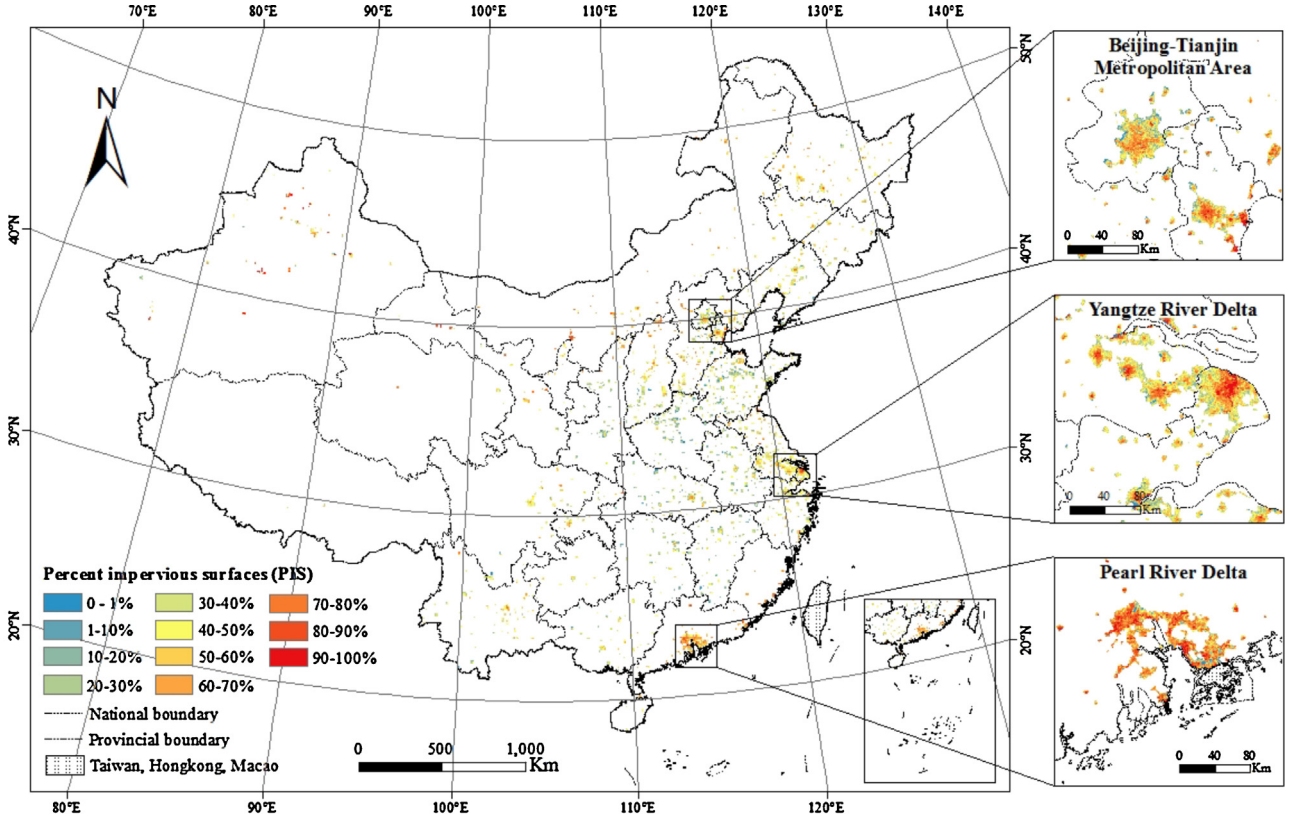

Fig. 4. Spatial distribution of urban IS in China in 2009.

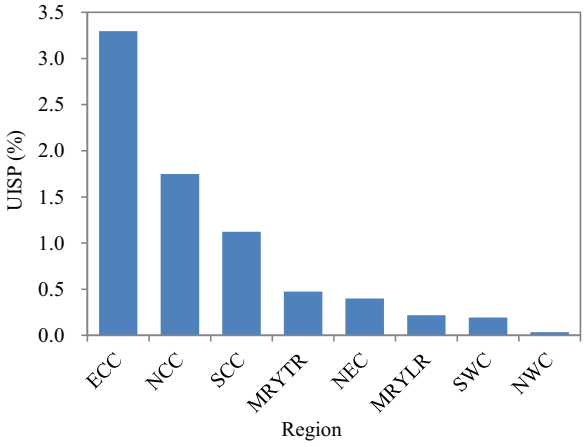

Fig. 5. Urban IS percentage (UISP) in different regions in 2009.

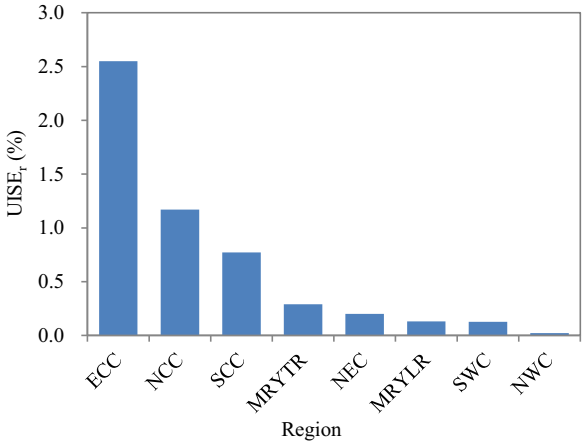

Fig. 7. The relative urban IS expansion index (UISE$_r$) in different regions from 1992 to 2009.

Urban IS expansion in China from 1992 to 2009 also showed large regional differences, with the exactly same pattern to that of UISP in 2009 (Fig. 7). These discrepancies in UISE$_r$ were even more pronounced at the provincial scale (Fig. 8). The UISE$_r$ of three metropolitan regions – Beijing, Tianjin, and Shanghai – were larger than 3%, whereas the UISE$_r$ of seven provinces (Sichuan, Guizhou, Inner Mongolia, Xinjiang, Gansu, Qinghai, and Tibet) were less than 0.1%. The total area of urban IS expansion from 1992 to 2009 in the three metropolitan regions was 2205.58 km^2, similar to the total area of urban IS expansion (2218.76 km^2) in the seven provinces covering 61.04% of China's total land area.

There were six large hotspot areas that experienced extremely rapid urban IS expansion in China from 1992 to 2009 (Fig. 9). Two hotspot areas, Beijing-Tianjin-Tangshan area and Qingdao area, were located in NCC. The other four hotspot areas, Yangtze River Delta, Pearl River Delta, Changsha-Xiangtan area, and Chengdu area, were distributed in ECC, SCC, MRYTR, and SWC, respectively. Among the hotspot areas, Pearl River Delta had the highest UISE$_r$ (11.28%), followed by Yangtze River Delta (10.54%) and Beijing-Tianjin-Tangshan area (8.07%). The UISE$_r$ in Chengdu area, Qingdao area, and Changsha-Xiangtan area ranged from 5% to 8%. The average of UISE$_r$ in the six hotspot areas was 7.98%, nearly 37 times the

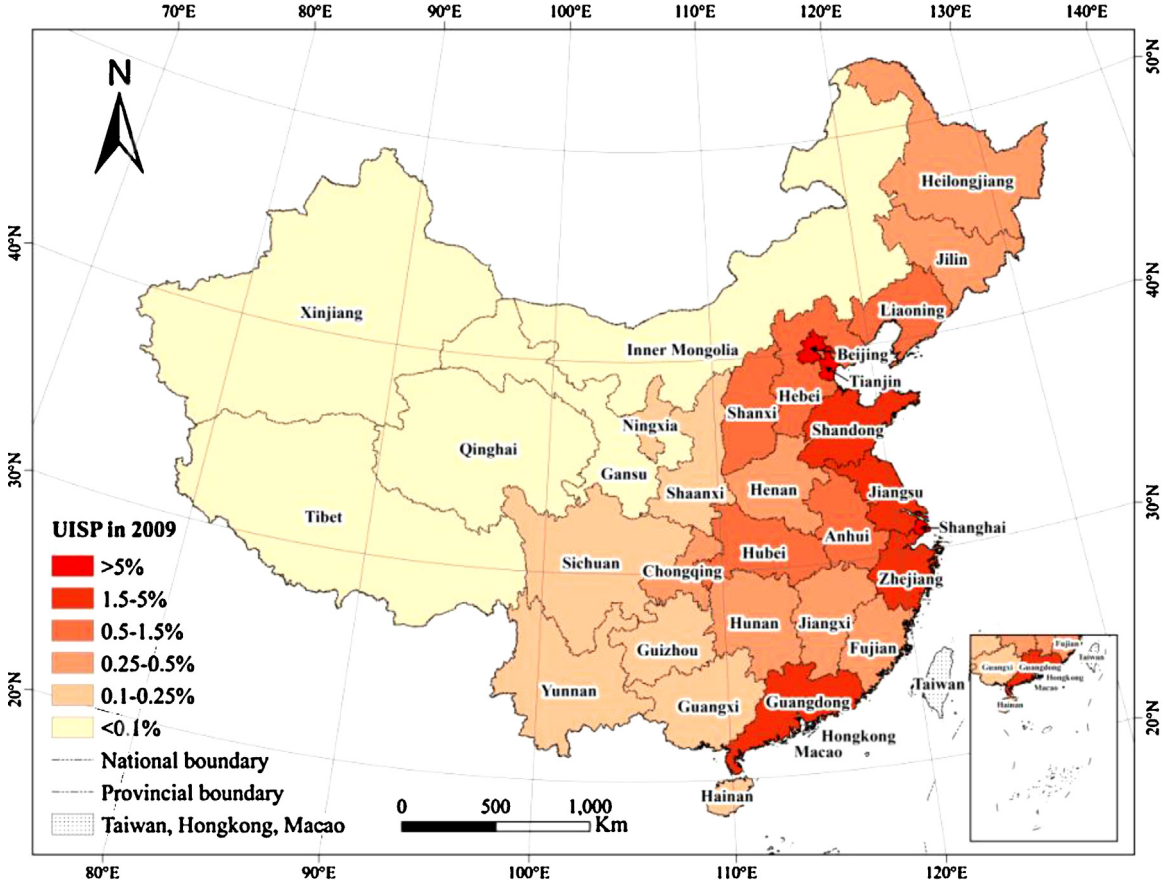

Fig. 6. UISP in different provinces in 2009.

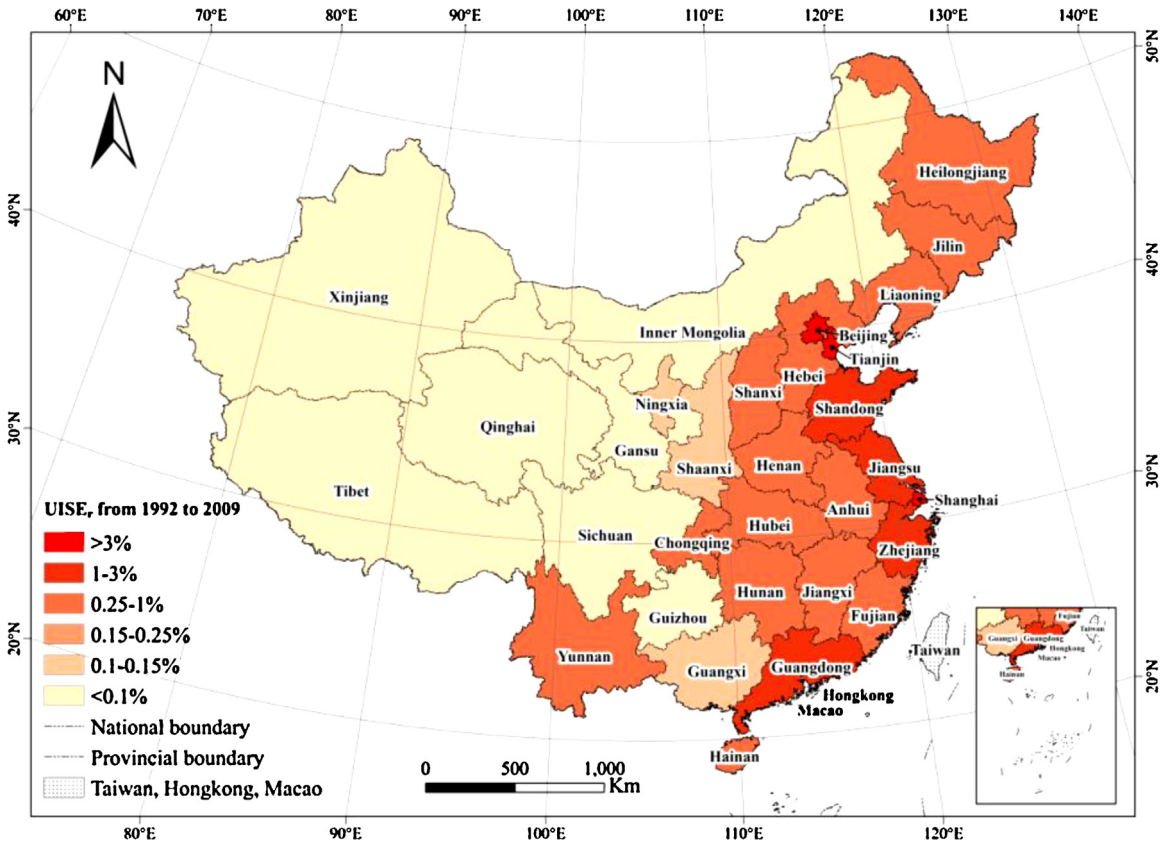

Fig. 8. The relative urban IS expansion index ($UISE_r$) in different provinces from 1992 to 2009.

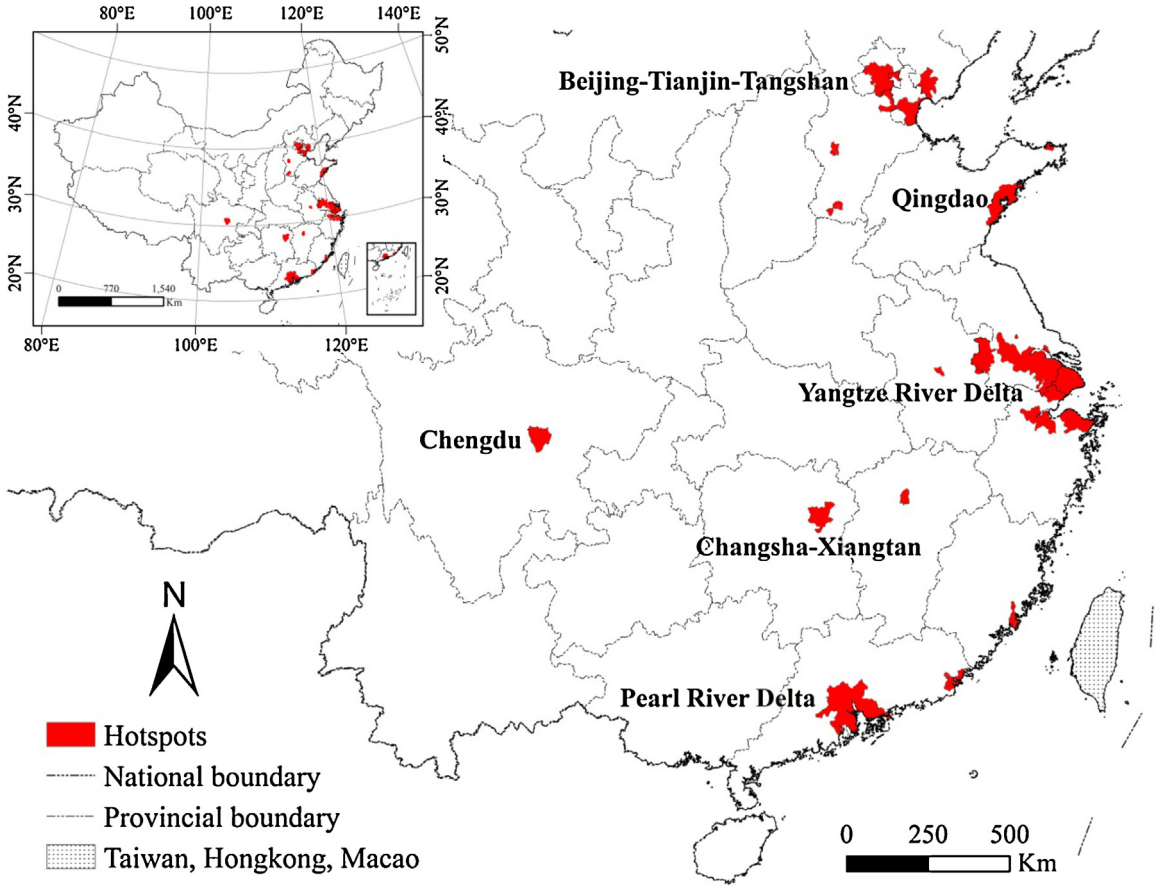

Fig. 9. Hotspot areas with high $UISE_r$ from 1992 to 2009.

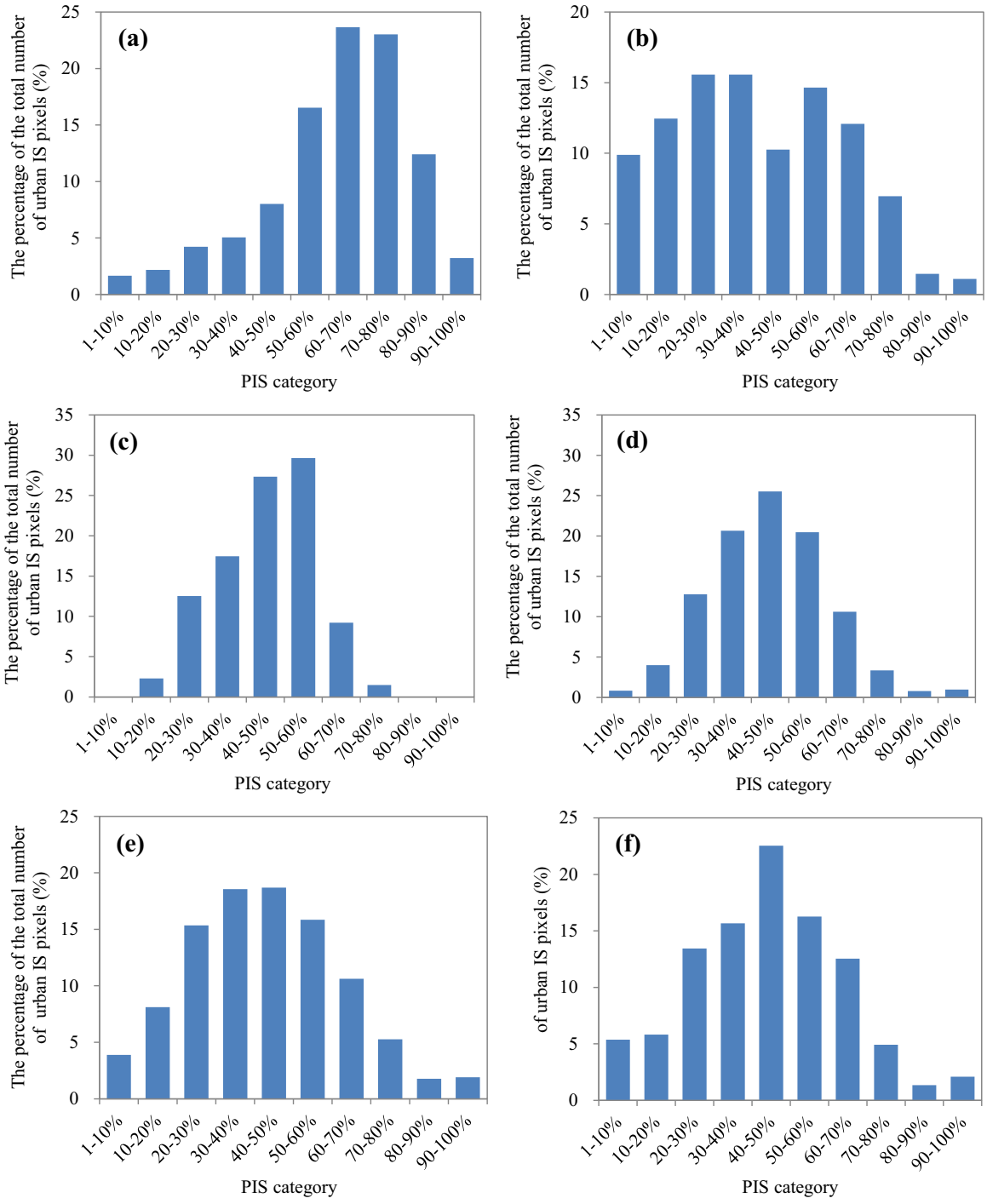

Fig. 10. The percentage of the total number of urban IS pixels categorized by 10% interval in new urban areas from 1992 to 2009 for the hotspot areas of Pearl River Delta (a), Changsha-Xiangtan (b), Chengdu (c), Yangtze River Delta (d), Beijing-Tianjin-Tangshan (e), and Qingdao (f).

national $UISE_r$ of China (0.22%). The six hotspot areas accounted for only 0.87% of China's total land area, but made up 37.66% of China's total area of urban IS expansion during 1992–2009.

The relative dominance of different types of urban IS expansion in new urban areas in terms of PIS varied among the hotspots areas (Fig. 10). The main type of urban IS expansion for Pearl River Delta was medium- and high-intensity urban IS, where the total number of urban IS pixels in the 50–90% PIS categories accounted for 75.62% of the total number of urban IS pixels in the new urban area (Fig. 10a). By contrast, most urban IS expansion in the new urban area for Changsha-Xiangtan area was of low-intensity, with the total number of urban IS pixels in the 1–40% PIS categories accounting for 53.48% of all urban IS pixels in the new urban area (Fig. 10b). Urban IS expansion for Chengdu area, Yangtze River Delta, Beijing-Tianjin-Tangshan area, and Qingdao area was dominated by medium- and low-intensity urban IS, with the total number of urban IS pixels in the 20–60% PIS categories accounting for 86.99%, 79.44%, 68.44%, and 67.91% of all urban IS pixels in the new urban area, respectively (Fig. 10c–f).

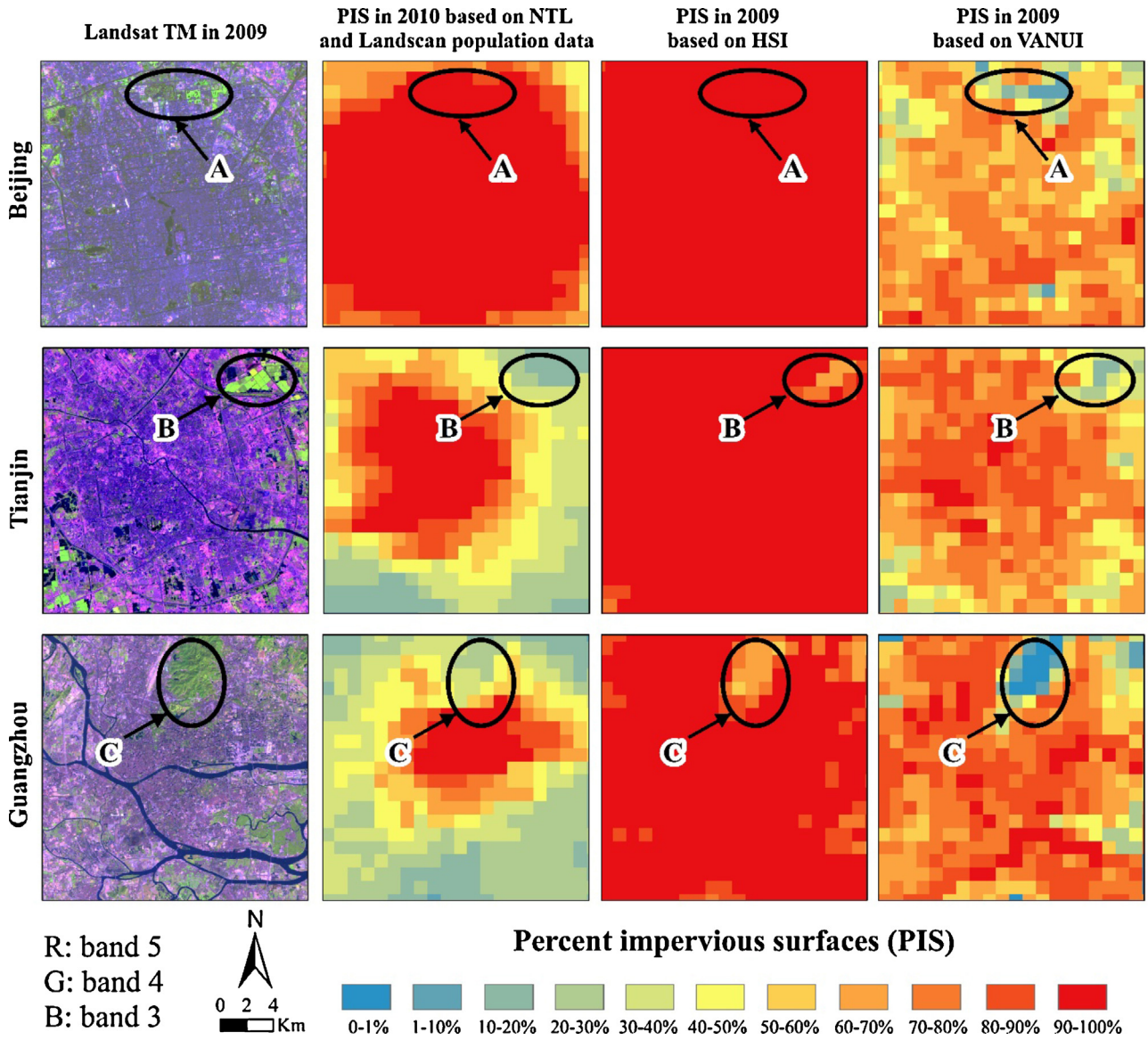

Fig. 11. Comparison of the estimated PIS based on VANUI in 2009, NTL and Landscan population data in 2010, and HSI in 2009 for the selected urban areas in reference to the Landsat TM data in 2009. The estimated PIS based on VANUI clearly identified the Olympic Forest Park in Beijing (A), farmland in Tianjin (B), and Baiyunshan Scenic Spot in Guangzhou (C).

5. Discussions

5.1. VANUI as an effective index for quantifying the spatiotemporal patterns of urban IS

Two methods have been used to quantify the IS of China based on the NTL data. The first is to calculate IS by combining radiance calibrated NTL data with Landscan population count data (Elvidge et al., 2007; Sutton et al., 2011). With this method, Elvidge et al. (2007) produced the first global inventory of the spatial distribution of PIS during 2000–2001. The major shortcoming of this global PIS product was that the calibration only included sites in the USA (Elvidge et al., 2010). However, because the intensity of the nighttime lighting and population density in China and the USA was quite different, the PIS of China in the global PIS product was not accurate. To overcome this problem, Sutton et al. (2011) used a Google Earth-based web application to collect the reference data derived from high-resolution images in China to validate the estimation of PIS in 2010. The result was still unsatisfactory for at least three reasons. First, there was an obvious saturation problem of PIS in urban

Table 2
Comparison of the average RMSE, MAE, SE, and *R* of the estimated PIS for eight regions based on NTL and Landscan population data in 2010, HSI in 2009, and VANUI in 2009.

	RMSE	MAE	SE	*R*
PIS in 2010 based on NTL and Landscan population data	0.275	0.236	−0.170	0.664
PIS in 2009 based on HSI	0.316	0.258	0.239	0.462
PIS in 2009 based on VANUI	0.128	0.105	−0.008	0.846

Note: RMSE represents root-mean-square error; MAE represents mean absolute error; SE represents systematic error; *R* represents correlation coefficient between the estimated PIS and the actual PIS.

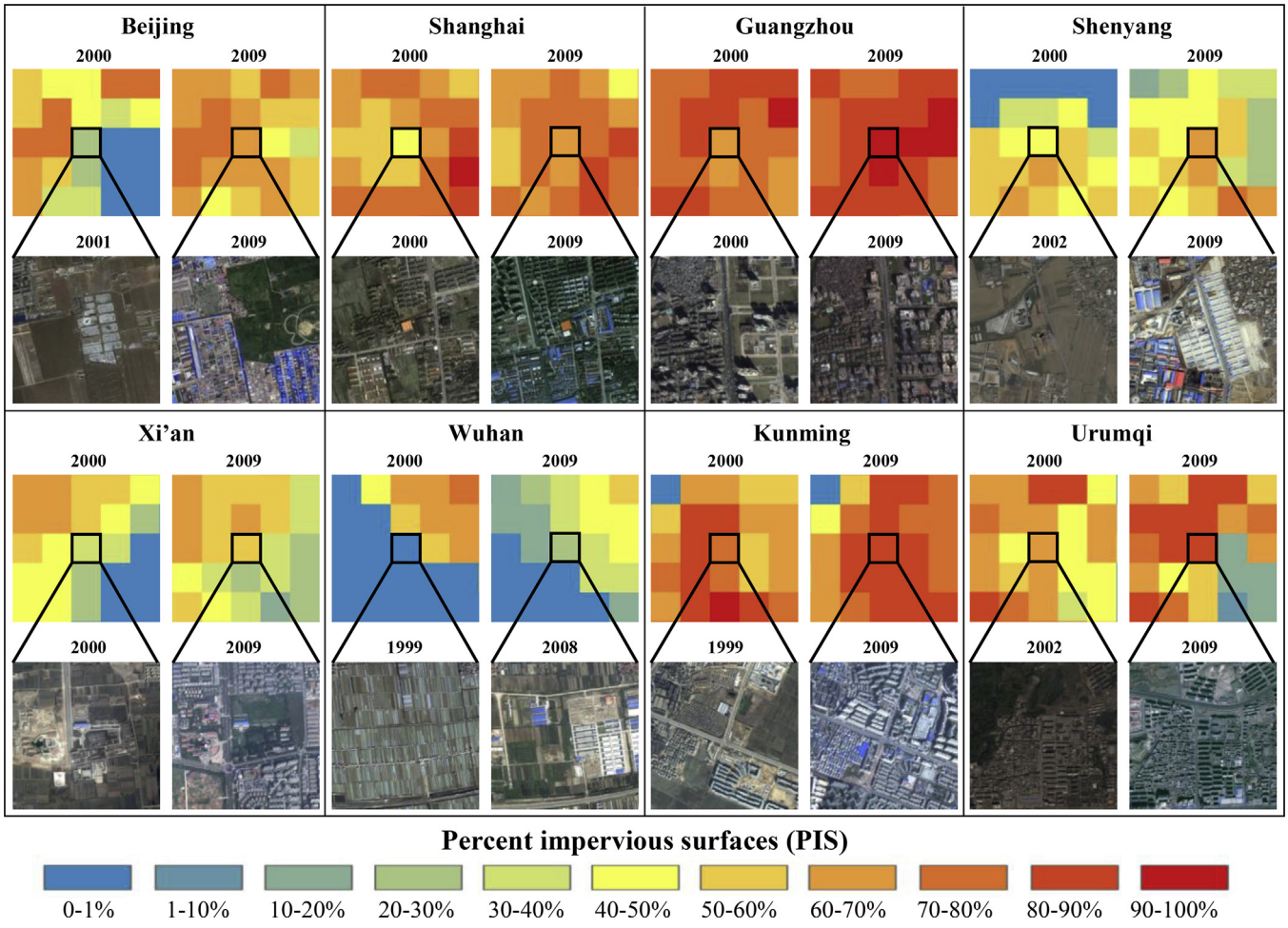

Fig. 12. Accuracy assessment of the estimated PIS dynamics based on VANUI from 2000 to 2009 for eight areas with a window size of 1 km × 1 km in reference to the high-resolution images in the corresponding years.

cores – PIS values of urban cores were always 100%, thus masking the spatial details of urban IS (Fig. 11). Second, PIS values of some regions in urban cores were considerably overestimated, as in the case of Olympic Forest Park in Beijing where the estimated PIS values were obviously larger than their actual ones (Fig. 11). Third, PIS values of regions immediately peripheral to urban cores were obviously underestimated. For example, the estimated PIS values outside the urban cores of Tianjin and Guangzhou were clearly lower than their actual ones (Fig. 11).

The second method is to estimate IS using Human Settlement Index (HSI) (Kuang et al., 2013). Like VANUI, HSI combines NTL and NDVI data, which can be an effective way of mapping human settlement at a regional scale (Lu et al., 2008). Kuang et al. (2013) mapped the spatiotemporal pattern of IS across China during 2000–2008

Table 3
Accuracy assessment of the estimated PIS based on VANUI for eight regions during 1992–2009.

Year	Index	NEC	NCC	ECC	SCC	MRYLR	MRYTR	SWC	NWC	Average
2009	RMSE	0.158	0.127	0.074	0.103	0.158	0.131	0.175	0.098	0.128
	MAE	0.115	0.103	0.063	0.090	0.116	0.111	0.154	0.082	0.105
	SE	0.031	−0.037	0.024	−0.019	0.049	0.029	−0.116	−0.023	−0.008
	R	0.840	0.871	0.885	0.871	0.892	0.809	0.819	0.783	0.846
2000	RMSE	0.175	0.159	0.062	0.095	0.147	0.137	0.143	0.101	0.127
	MAE	0.116	0.126	0.046	0.086	0.108	0.115	0.107	0.079	0.098
	SE	0.040	−0.058	0.013	−0.015	−0.001	0.065	−0.083	−0.058	−0.012
	R	0.817	0.932	0.918	0.928	0.888	0.879	0.907	0.748	0.877
1992	RMSE	0.160	0.189	0.117	0.170	0.155	0.177	0.172	0.086	0.154
	MAE	0.112	0.158	0.083	0.134	0.120	0.140	0.142	0.072	0.120
	SE	0.016	−0.070	−0.033	0.001	0.003	−0.038	−0.095	−0.060	−0.035
	R	0.840	0.796	0.873	0.759	0.868	0.811	0.796	0.912	0.832
Average	RMSE	0.164	0.158	0.085	0.123	0.153	0.148	0.164	0.095	0.136
	MAE	0.115	0.129	0.064	0.103	0.115	0.122	0.135	0.078	0.108
	SE	0.029	−0.055	0.001	−0.011	0.017	0.019	−0.098	−0.047	−0.018
	R	0.832	0.866	0.892	0.852	0.883	0.833	0.841	0.814	0.852

by directly equating PIS to HSI. However, estimating PIS directly from HSI is problematic because most values of HSI in urban area are larger than 1, resulting in the saturation problem again (Fig. 11). Also, PIS values of urban areas are often overestimated, as illustrated by farmlands in Tianjin and Baiyunshan Scenic Spot in Guangzhou where PIS values were all above 60% (Fig. 11). In addition, deriving HSI without preprocessing NTL data for different years is not desirable for quantifying urban IS dynamics because the NTL data are incompatible between years (Liu, He, et al., 2012; Zhao et al., 2012).

In contrast, VANUI is more intuitive and simpler to implement, and more strongly correlated with PIS than HSI (Zhang et al., 2013). Our results further supported this claim as the estimated urban PIS using VANUI accurately identified not only the regions with high PIS but also those with low PIS (e.g., farmland and Baiyunshan Scenic Spot). Also, our study with VANUI substantially improved the estimation accuracy of urban IS in comparison to the other two methods (Table 2). The average RMSE, MAE, and SE for eight regions based on VANUI in 2009 were 0.128, 0.105, and −0.008, respectively, which were obviously less than the corresponding values based on the other two methods (Table 2). The avaerage R based on VANUI in 2009 amounted to 0.846, while the average R based on the other two methods were all less than 0.664 (Table 2).

In addition, the average RMSE for the whole study area from 1992 to 2009 was 0.136, with MAE of 0.108, SE of −0.018, and R of 0.852 (Table 3). We also assessed the accuracy of detected changes in urban PIS for eight small areas with a window size of 1 km × 1 km, located in Beijing, Shanghai, Guangzhou, Shenyang, Xi'an, Wuhan, Kunming, and Urumqi (Fig. 12). For example, the estimated urban PIS within the sample area (1 km^2) in 2000 and 2009 were 28.68% and 64.25% for Beijing, 69.25% and 93.47% for Guangzhou, 0% and 27.72% for Wuhan, and 69.55% and 82.85% for Urumqi. These urban PIS estimates all corresponded well with the characteristics of urban PIS dynamics presented in the corresponding high-resolution images (Fig. 12).

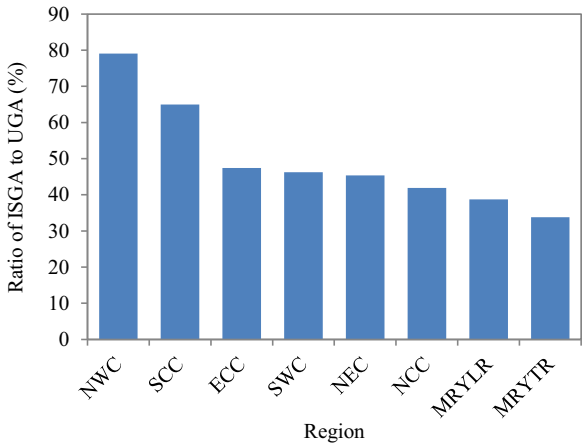

Fig. 13. Ratio of impervious surfaces growth area (ISGA) to urban growth area (UGA) in different regions from 1992 to 2009.

5.2. Urban IS as an indicator for monitoring urban expansion

Urban IS may serve as an important indicator of urbanization and its environmental impacts (Arnold & Gibbons, 1996; Weng, 2012). In comparison with other measures of urbanized area, urban IS can more precisely characterize urban environment (Powell, Cohen, Yang, Pierce, & Alberti, 2008) and capture the details of urban expansion (Xian & Homer, 2010). Therefore, urban IS have been widely used in monitoring the dynamics of urban expansion (Gao et al., 2012; Zhou, He, Nigh, & Schulz, 2012).

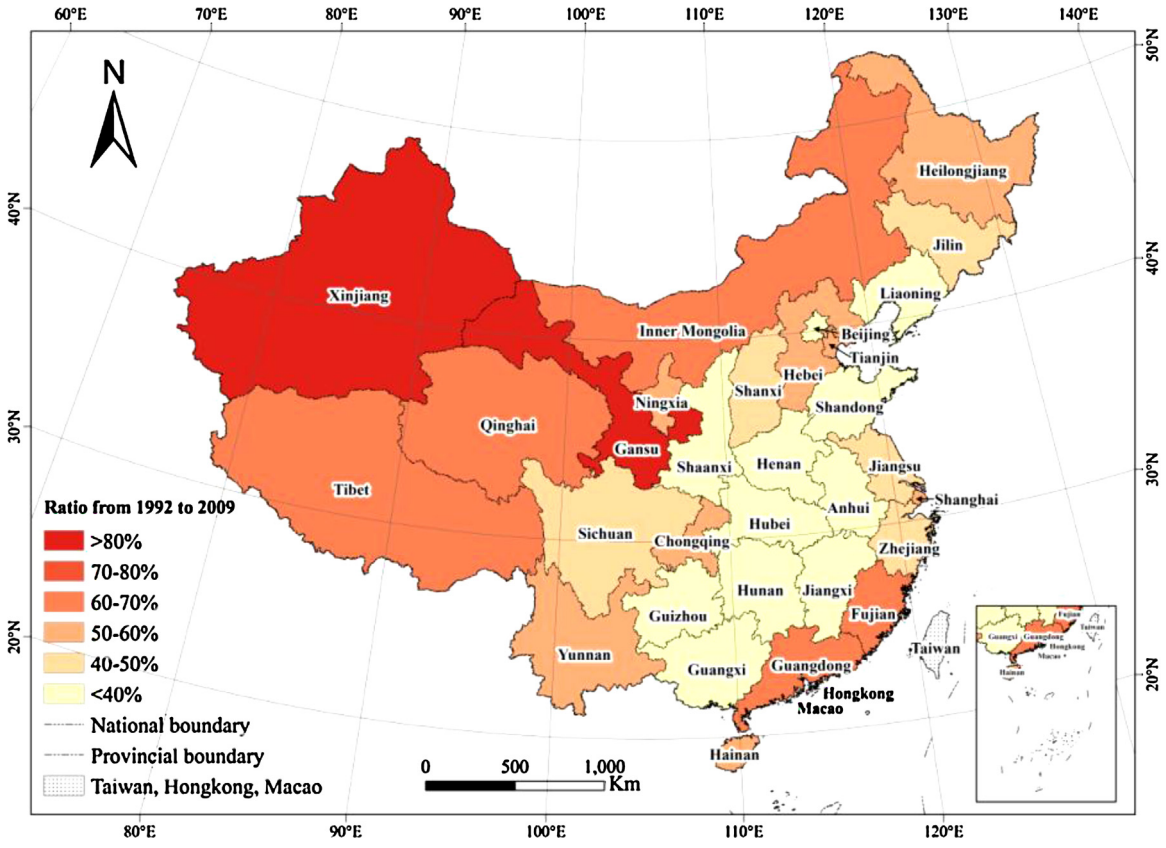

Fig. 14. Ratio of ISGA to UGA in different provinces from 1992 to 2009.

In this study, we calculated the ratio of impervious surfaces growth area (ISGA) to urban growth area (UGA) at the regional and provincial scales to characterize the dynamics of urban expansion in China for 1992–2009. Our results indicated that there were clearly regional differences in urban expansion in China from 1992 to 2009. The ratios in NWC and SCC were 79.04% and 64.93%, respectively, which were substantially larger than the values in other regions (Fig. 13). These relatively high ratios suggested most urban expansion in NWC and SCC was associated with relatively high-intensity urban IS development. The ratios in ECC, SWC, NEC, and NCC ranged from 40% to 50%, indicating the urban expansion in these regions was dominated by medium-intensity urban IS development. By contrast, MRYLR and MRYTR had relatively low ratios (less than 40%), indicating large areas of low-intensity urban IS in their new urban areas for 1992–2009. The discrepancies in the ratio were more noticeable at the provincial scale (Fig. 14). The ratios in Xinjiang and Gansu were all larger than 80%, suggesting the urban development in these two provinces from 1992 to 2009 was relatively compact. The lowest ratio (20.41%) occurred in Henan, followed by Shaanxi (26.33%) and Hunan (30.14%). The lower ratios of ISGA/UGA were correlated with low-intensity urban development, which usually have broader negative impacts on the environment.

5.3. Limitations and future directions

Our study has a few limitations that need to be addressed in future research. For example, because the approach that we used here is based on the regression analysis, the number and quality of samples will influence the robustness of the regression model and thus the accuracy of the final outcome. Also, the PIS of water bodies in urban areas was overestimated due to their high NTL and low NDVI values (e.g., Guangzhou in Fig. 11).

In our future studies, we will look into the detailed relationship between urban IS and related indices to reduce uncertainties and increase estimation accuracy. In addition, we will analyze the relationship between urban IS and ecological variables to investigate the impacts of urbanization on the environment.

6. Conclusions

In this study, we quantified the spatiotemporal patterns of urban IS of China from 1992 to 2009 using the VANUI index, with a higher accuracy than other existing studies. Our results indicate that the total urban impervious surface area of China increased rapidly from 1992 to 2009 at a rate of 6.54% per year, with large regional differences in space and time. For example, in 2009 more than half of the total impervious surface area (54.64%) came from three coastal regions that accounted for only 9.63% of the total land area of China. Also, we identified six large hotspot areas with high impervious surface expansion rates which exhibited different ways of adding new impervious surfaces. The main type of urban impervious surface expansion was medium- and high-intensity (50–90%) for Pearl River Delta, low-intensity (1–40%) for Changsha-Xiangtan area, and medium- and low-intensity (20–60%) for Chengdu area, Yangtze River Delta, Beijing-Tianjin-Tangshan area, and Qingdao area. The ratio of ISGA/UGA can effectively characterize the dynamics of urban expansion. Our results should be valuable for further understanding environmental impacts of urbanization and for sustainable urban planning and management in China and beyond.

Acknowledgements

We would like to express our respects and gratitude to the anonymous reviewers and editors for their valuable comments and suggestions on improving the quality of the paper. Our research was supported in part by the National Basic Research Programs of China (Grant Nos. 2014CB954302, 2014CB954303 and 2010CB950901) and the National Natural Science Foundation of China (Grant No. 41222003).

References

Amaral, S., Câmara, G., Monteiro, A. M. V., Quintanilha, J. A., & Elvidge, C. D. (2005). Estimating population and energy consumption in Brazilian Amazonia using DMSP night-time satellite data. *Computers, Environment and Urban Systems*, *29*(2), 179–195.

Anselin, L. (1995). Local indicators of spatial association—LISA. *Geographical analysis*, *27*(2), 93–115.

Arnold, C. L., & Gibbons, C. J. (1996). Impervious surface coverage – The emergence of a key environmental indicator. *Journal of the American Planning Association*, *62*(2), 243–258.

Bai, X., Chen, J., & Shi, P. (2012). Landscape urbanization and economic growth in China: Positive feedbacks and sustainability dilemmas. *Environmental Science & Technology*, *46*(1), 132–139.

Brabec, E. (2002). Impervious surfaces and water quality: A review of current literature and its implications for watershed planning. *Journal of planning literature*, *16*(4), 499–514.

Buyantuyev, A., & Wu, J. (2010). Urban heat islands and landscape heterogeneity: Linking spatiotemporal variations in surface temperatures to land-cover and socioeconomic patterns. *Landscape Ecology*, *25*(1), 17–33.

Cao, X., Chen, J., Imura, H., & Higashi, O. (2009). A SVM-based method to extract urban areas from DMSP-OLS and SPOT VGT data. *Remote Sensing of Environment*, *113*(10), 2205–2209.

Deng, Y., Fan, F., & Chen, R. (2012). Extraction and analysis of impervious surfaces based on a spectral un-mixing method using pearl river delta of China Landsat TM/ETM+ imagery from 1998 to 2008. *Sensors*, *12*(2), 1846–1862.

Development Research Center of the State Council of China. (2005). Coordinated Regional Development Strategy and Policy Reports. (in Chinese).

Doll, C. N. H., Muller, J. P., & Elvidge, C. D. (2000). Night-time imagery as a tool for global mapping of socioeconomic parameters and greenhouse gas emissions. *AMBIO: A Journal of the Human Environment*, *29*(3), 157–162.

Elvidge, C. D., Baugh, K. E., Dietz, J. B., Bland, T., Sutton, P. C., & Kroehl, H. W. (1999). Radiance calibration of DMSP-OLS low-light imaging data of human settlements. *Remote Sensing of Environment*, *68*(1), 77–88.

Elvidge, C. D., Baugh, K. E., Kihn, E. A., Kroehl, H. W., & Davis, E. R. (1997). Mapping city lights with nighttime data from the DMSP Operational Linescan System. *Photogrammetric Engineering and Remote Sensing*, *63*(6), 727–734.

Elvidge, C. D., Imhoff, M. L., Baugh, K. E., Hobson, V. R., Nelson, I., Safran, J., et al. (2001). Night-time lights of the world: 1994–1995. *ISPRS Journal of Photogrammetry and Remote Sensing*, *56*(2), 81–99.

Elvidge, C. D., Milesi, C., Dietz, J. B., Tuttle, B. T., Sutton, P. C., Nemani, R., et al. (2004). US constructed area approaches the size of Ohio. *EOS, Transactions American Geophysical Union*, *85*(24), 233–234.

Elvidge, C. D., Tuttle, B. T., & Sutton, P. C. (2010). Collaborative tool for collecting reference data on the density of constructed surfaces worldwide. In *Sixth International Symposium on Digital Earth: Models, Algorithms, and Virtual Reality, 7840* (pp. 1–8).

Elvidge, C. D., Tuttle, B. T., Sutton, P. S., Baugh, K. E., Howard, A. T., Milesi, C., et al. (2007). Global distribution and density of constructed impervious surfaces. *Sensors*, *7*(9), 1962–1979.

Fensholt, R., Rasmussen, K., Theis, T., & Mbow, C. (2009). Evaluation of earth observation based long term vegetation trends—Intercomparing NDVI time series trend analysis consistency of Sahel from AVHRR GIMMS, Terra MODIS and SPOT VGT data. *Remote Sensing of Environment*, *113*, 1886–1898.

Gallo, K., Ji, L., Reed, B., Dwyer, J., & Eidenshink, J. (2004). Comparison of MODIS and AVHRR 16-day normalized difference vegetation index composite data. *Geophysical Research Letters*, *31*(7)

Gao, F., de Colstoun, E. B., Ma, R., Weng, Q., Masek, J. G., Chen, J., et al. (2012). Mapping impervious surface expansion using medium-resolution satellite image time series: A case study in the Yangtze River Delta, China. *International Journal of Remote Sensing*, *33*(24), 7609–7628.

Goetz, S., & Fiske, G. (2008). Linking the diversity and abundance of stream biota to landscapes in the mid-Atlantic USA. *Remote Sensing of Environment*, *112*(11), 4075–4085.

Goodchild, M. F. (1986). *Spatial autocorrelation*. Norwich: Geo Books.

Gu, J., Li, X., Huang, C., & Okin, G. S. (2009). A simplified data assimilation method for reconstructing time-series MODIS NDVI data. *Advances in Space Research*, *44*(4), 501–509.

He, C., Ma, Q., Liu, Z., & Zhang, Q. (2013). Modeling the spatiotemporal dynamics of electric power consumption in Mainland China using saturation-corrected DMSP/OLS nighttime stable light data. *International Journal of Digital Earth*, 1–22 (Epub ahead of print).

Henderson, M., Yeh, E. T., Gong, P., Elvidge, C., & Baugh, K. (2003). Validation of urban boundaries derived from global night-time satellite imagery. *International Journal of Remote Sensing*, *24*(3), 595–609.

Holben, B. N. (1986). Characteristics of maximum-value composite images from temporal AVHRR data. *International Journal of Remote Sensing*, *7*(11), 1417–1434.

Hu, X., & Weng, Q. (2009). Estimating impervious surfaces from medium spatial resolution imagery using the self-organizing map and multi-layer perceptron neural networks. *Remote Sensing of Environment*, *113*(10), 2089–2102.
Huete, A., Didan, K., Miura, T., Rodriguez, E. P., Gao, X., & Ferreira, L. G. (2002). Overview of the radiometric and biophysical performance of the MODIS vegetation indices. *Remote Sensing of Environment*, *83*(1), 195–213.
Imhoff, M. L., Lawrence, W. T., Stutzer, D. C., & Elvidge, C. D. (1997). A technique for using composite DMSP/OLS city lights satellite data to map urban area. *Remote Sensing of Environment*, *61*(3), 361–370.
Kuang, W., Liu, J., Zhang, Z., Lu, D., & Xiang, B. (2013). Spatiotemporal dynamics of impervious surface areas across China during the early 21st century. *Chinese Science Bulletin*, *58*(14), 1691–1701.
Leinenkugel, P., Esch, T., & Kuenzer, C. (2011). Settlement detection and impervious surface estimation in the Mekong Delta using optical and SAR remote sensing data. *Remote Sensing of Environment*, *115*(12), 3007–3019.
Liu, J., Liu, M., Zhuang, D., Zhang, Z., & Deng, X. (2003). Study on spatial pattern of land-use change in China during 1995–2000. *Science in China Series D: Earth Sciences*, *46*(4), 373–384.
Liu, J., Zhang, Q., & Hu, Y. (2012). Regional differences of China's urban expansion from late 20th to early 21st century based on remote sensing information. *Chinese Geographical Science*, *22*(1), 1–14.
Liu, Z., He, C., Zhang, Q., Huang, Q., & Yang, Y. (2012). Extracting the dynamics of urban expansion in China using DMSP-OLS nighttime light data from 1992 to 2008. *Landscape and Urban Planning*, *106*(1), 62–72.
Lo, C. (2001). Modeling the population of China using DMSP operational linescan system nighttime data. *Photogrammetric Engineering and Remote Sensing*, *67*(9), 1037–1047.
Lu, D., Tian, H., Zhou, G., & Ge, H. (2008). Regional mapping of human settlements in southeastern China with multisensor remotely sensed data. *Remote Sensing of Environment*, *112*(9), 3668–3679.
Lu, D., & Weng, Q. (2006). Use of impervious surface in urban land-use classification. *Remote Sensing of Environment*, *102*(1), 146–160.
Ma, T., Zhou, C., Pei, T., Haynie, S., & Fan, J. (2012). Quantitative estimation of urbanization dynamics using time series of DMSP/OLS nighttime light data: A comparative case study from China's cities. *Remote Sensing of Environment*, *124*, 99–107.
Milesi, C., Elvidge, C. D., Nemani, R. R., & Running, S. W. (2003). Assessing the impact of urban land development on net primary productivity in the southeastern United States. *Remote Sensing of Environment*, *86*(3), 401–410.
Ministry of Housing and Urban-Rural Development of China. (2012). *China Urban Construction Statistical Yearbook 2011*. Beijing: China Planning Press (in Chinese).
National Bureau of Statistics of China. (2012). *China Statistical Yearbook 2011*. Beijing: China Statistics Press (in Chinese).
Oke, T. R. (1982). The energetic basis of the urban heat island. *Quarterly Journal of the Royal Meteorological Society*, *108*(455), 1–24.
Pappas, E., Smith, D., Huang, C., Shuster, W., & Bonta, J. (2008). Impervious surface impacts to runoff and sediment discharge under laboratory rainfall simulation. *Catena*, *72*(1), 146–152.
Potere, D., & Schneider, A. (2007). A critical look at representations of urban areas in global maps. *GeoJournal*, *69*(1–2), 55–80.
Powell, S. L., Cohen, W. B., Yang, Z., Pierce, J. D., & Alberti, M. (2008). Quantification of impervious surface in the Snohomish Water Resources Inventory Area of Western Washington from 1972–2006. *Remote Sensing of Environment*, *112*(4), 1895–1908.
Sexton, J. O., Song, X., Huang, C., Channan, S., Baker, M. E., & Townshend, J. R. (2013). Urban growth of the Washington, D.C. – Baltimore, MD metropolitan region from 1984 to 2010 by annual, Landsat-based estimates of impervious cover. *Remote Sensing of Environment*, *129*, 42–53.
Shao, M., Tang, X., Zhang, Y., & Li, W. (2006). City clusters in China: Air and surface water pollution. *Frontiers in Ecology and the Environment*, *4*(7), 353–361.
Solano, R., Didan, K., Jacobson, A., & Huete, A. (2010). *MODIS vegetation indices (MOD13) C5 user's guide*. Tucson: The University of Arizona.
Steven, M. D., Malthus, T. J., Baret, F., Xu, H., & Chopping, M. J. (2003). Intercalibration of vegetation indices from different sensor systems. *Remote Sensing of Environment*, *88*(4), 412–422.
Sutton, P. C., Elvidge, C. D., Baugh, K., & Ziskin, D. (2011). Mapping the constructed surface area density for China. In *Proceedings of the 31st Asia-Pacific Advanced Network Meeting* (pp. 70–79).
Sutton, P. C., Elvidge, C. D., Tuttle, B. T., & Ziskin, D. (2010). A 2010 mapping of the constructed surface area density for S.E. Asia – Preliminary results. In *Proceedings of the 30st Asia-Pacific Advanced Network Meeting* (pp. 182–190).
Tan, M., Li, X., Xie, H., & Lu, C. (2005). Urban land expansion and arable land loss in China—A case study of Beijing–Tianjin–Hebei region. *Land Use Policy*, *22*(3), 187–196.
Tarnavsky, E., Garrigues, S., & Brown, M. E. (2008). Multiscale geostatistical analysis of AVHRR, SPOT-VGT, and MODIS global NDVI products. *Remote Sensing of Environment*, *112*, 535–549.
Teillet, P., & Holben, B. (1994). Towards operational radiometric calibration of NOAA AVHRR imagery in the visible and near-infrared channels. *Canadian Journal of Remote Sensing*, *20*(1), 1–10.
Wang, L., Li, C., Ying, Q., Cheng, X., Wang, X., Li, X., et al. (2012). China's urban expansion from 1990 to 2010 determined with satellite remote sensing. *Chinese Science Bulletin*, *57*(22), 2802–2812.
Weng, Q. (2001). Modeling urban growth effects on surface runoff with the integration of remote sensing and GIS. *Environmental Management*, *28*(6), 737–748.
Weng, Q. (2012). Remote sensing of impervious surfaces in the urban areas: Requirements, methods, and trends. *Remote Sensing of Environment*, *117*, 34–49.
Weng, Q., & Lu, D. (2008). A sub-pixel analysis of urbanization effect on land surface temperature and its interplay with impervious surface and vegetation coverage in Indianapolis, United States. *International Journal of Applied Earth Observation and Geoinformation*, *10*(1), 68–83.
Wu, C., & Murray, A. T. (2003). Estimating impervious surface distribution by spectral mixture analysis. *Remote Sensing of Environment*, *84*(4), 493–505.
Wu, J. (2010). Urban sustainability: An inevitable goal of landscape research. *Landscape Ecology*, *25*(1), 1–4.
Wu, J. (2014). Urban ecology and sustainability: The state-of-the-science and future directions. *Landscape and Urban Planning*, *125*, 209–221.
Wu, J., Buyantuyev, A., Jenerette, G. D., Litteral, J., Neil, K., & Shen, W. (2011). Quantifying spatiotemporal patterns and ecological effects of urbanization: A multiscale landscape approach. In M. Richter, & U. Weiland (Eds.), *Applied Urban Ecology: A Global Framework* (pp. 35–53). Blackwell. http://dx.doi.org/10.1002/9781444345025.ch4
Wu, J., Xiang, W., & Zhao, J. (2014). Urban ecology in China: Historical developments and future directions. *Landscape and Urban Planning*, *125*, 222–233.
Xian, G., & Homer, C. (2010). Updating the 2001 national land cover database impervious surface products to 2006 using Landsat imagery change detection methods. *Remote Sensing of Environment*, *114*(8), 1676–1686.
Yang, Y., He, C., Zhang, Q., Han, L., & Du, S. (2013). Timely and accurate national-scale mapping of urban land in China using Defense Meteorological Satellite Program's Operational Linescan System nighttime stable light data. *Journal of Applied Remote Sensing*, *7*(1), 073535.
Zhang, Q., Schaaf, C., & Seto, K. C. (2013). The Vegetation Adjusted NTL Urban Index: A new approach to reduce saturation and increase variation in nighttime luminosity. *Remote Sensing of Environment*, *129*, 32–41.
Zhao, N., Ghosh, T., & Samson, E. L. (2012). Mapping spatio-temporal changes of Chinese electric power consumption using night-time imagery. *International Journal of Remote Sensing*, *33*(20), 6304–6320.
Zhao, S., Da, L., Tang, Z., Fang, H., Song, K., & Fang, J. (2006). Ecological consequences of rapid urban expansion: Shanghai, China. *Frontiers in Ecology and the Environment*, *4*(7), 341–346.
Zhou, B., He, H. S., Nigh, T. A., & Schulz, J. H. (2012). Mapping and analyzing change of impervious surface for two decades using multi-temporal Landsat imagery in Missouri. *International Journal of Applied Earth Observation and Geoinformation*, *18*, 195–206.
Zhou, L., Dickinson, R. E., Tian, Y., Fang, J., Li, Q., Kaufmann, R. K., et al. (2004). Evidence for a significant urbanization effect on climate in China. *Proceedings of the National Academy of Sciences of the United States of America*, *101*(26), 9540–9544.
Zhou, Y., Smith, S. J., Elvidge, C. D., Zhao, K., Thomson, A., & Imhoff, M. (2014). A cluster-based method to map urban area from DMSP/OLS nightlights. *Remote Sensing of Environment*, *147*, 173–185.